

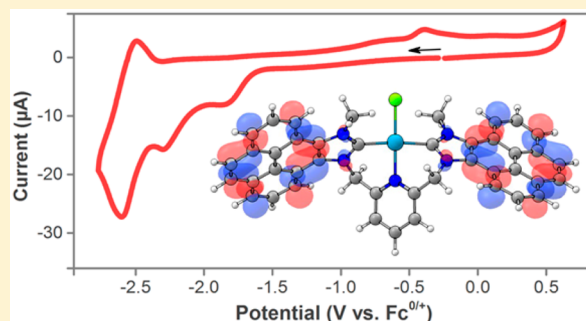
Polyannulated Bis(N-heterocyclic carbene)palladium Pincer Complexes for Electrocatalytic CO₂ Reduction

Jeffrey A. Therrien, Michael O. Wolf,* and Brian O. Patrick

Department of Chemistry, University of British Columbia, Vancouver, British Columbia V6T 1Z1, Canada

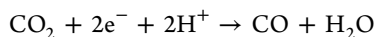
Supporting Information

ABSTRACT: Phenanthro- and pyrene-annulated N-heterocyclic carbenes (NHCs) have been incorporated into lutidine-linked bis-NHC Pd pincer complexes to investigate the effect of these polyannulated NHCs on the ability of the complexes to electrochemically reduce CO₂ to CO in the presence of 2,2,2-trifluoroacetic acid and 2,2,2-trifluoroethanol as proton sources. These complexes are screened for their ability to reduce CO₂ and modeled using density functional theory calculations, where the annulated phenanthrene and pyrene moieties are shown to be additional sites for redox activity in the pincer ligand, enabling increased electron donation. Electrochemical and computational studies are used to gain an understanding of the chemical significance of redox events for complexes of this type, highlighting the importance of anion binding and dissociation.

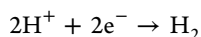


INTRODUCTION

There is currently great interest in developing more efficient ways to use CO₂ as a chemical feedstock for the production of renewable fuels and value-added chemicals.^{1–3} Hydrocarbon fuels are advantageous because of their ability to be stable, long-term energy storage materials with higher energy densities than batteries.⁴ The two-electron reduction of CO₂ to produce CO can be coupled with Fischer–Tropsch chemistry to produce long-chain liquid hydrocarbon fuels, creating a closed CO₂ cycle for combustion processes.⁴



$$E^\circ = -0.53 \text{ V at pH 7 vs NHE}$$



$$E^\circ = -0.42 \text{ V at pH 7 vs NHE}$$

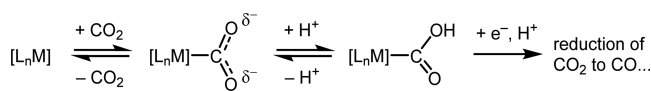
The use of homogeneous molecular electrocatalysts to enable the reduction of CO₂ to CO is an attractive approach because the properties of the electrocatalyst can be tuned through ligand modification and well-defined complexes can be studied in solution, allowing a greater understanding of the mechanism of the reaction with CO₂ to be attained. Research into CO₂ reduction electrocatalysts has progressed since early discoveries in the 1980s, although a robust understanding of the design factors required for highly selective CO₂ reduction over H⁺ reduction, an inherently competitive reaction because of the requirement of protons in the reduction of CO₂, is still developing.^{3,5,6} Previous investigations probing the structure–activity relationships of phosphine-containing palladium pincer electrocatalysts found that selectivity for CO₂ reduction was extremely sensitive to variations in the ligand substituents,

donor type, bite angle, and changes in the redox potential of the complex. These factors can act to modify the basicity of a catalytic complex and the energy and stability of hydride formation, leading to subsequent hydrogen production.^{7,8} In general, less negative reduction potentials have been found to be beneficial for improved selectivity for CO₂ reduction.

High selectivity for CO₂ reduction can also be achieved at more reducing potentials if the active electrocatalyst species can activate CO₂ to a sufficiently high degree, resulting in negative charge formation on the oxygen atoms of the bound CO₂ and higher basicity than the metal center. Density functional theory (DFT) analysis of the bonding energy and degree of CO₂ activation for the electrocatalysts Re(bpy)(CO)₃Cl and [Pd-(triposphine)(CH₃CN)]²⁺ show energetically favorable binding and activation of CO₂ with O–C–O bond angles of approximately 123° and 130°, respectively, at their energy minima, which allow the use of water and HBF₄, respectively, as weakly and strongly acidic proton sources.^{6,9–11} The greater degree of CO₂ activation achieved with Re(bpy)(CO)₃Cl allows the use of weak acid sources at highly reducing potentials while avoiding H₂ production because the half-cell potential for H⁺ reduction becomes more negative with increasing pK_a.¹² Conversely, a lower degree of CO₂ activation requires the use of stronger, less discriminating Brønsted acids for protonation of the bound CO₂ and subsequent catalytic turnover (Scheme 1). Additionally, if a strong acid is required, the catalyst should operate at low potentials to limit background H⁺ reduction at the working electrode, which can occur at the electrode surface even in the absence of electrocatalyst at rates that increase

Received: July 28, 2015

Scheme 1. Proposed Equilibria for Protonation of Activated CO₂



exponentially with applied overpotential when mass transport is not limiting.¹²

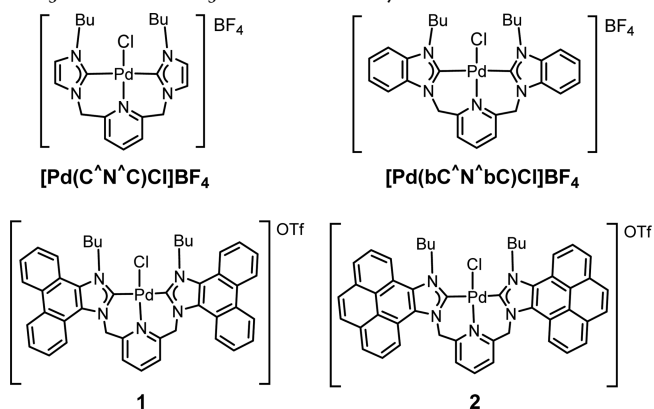
Redox-active ligands have a promising role in the design of improved CO₂ reduction electrocatalysts because they can store at least some of the charge required for CO₂ activation away from the metal center, reducing the basicity of the reduced complex. This is showcased prominently in M(bpy)(CO)₃X-type complexes (where M = Mn or Re)^{13,14} and is an important factor in previous work from our group where lutidyl-linked bis(N-heterocyclic carbene) Pd pincer complexes were found to reduce CO₂ to CO at moderate potentials with trifluoroacetic acid [TFA; pK_a = 3.5 in dimethyl sulfoxide (DMSO)¹⁵] as the proton source.¹⁰ One mitigating factor for the performance of these bis-NHC electrocatalysts is the direct reduction of H⁺ at the electrode surface, accounting for up to half of the current passed at typical operating potentials.

With this general bis-NHC ligand framework, less negative reduction potentials and improved selectivity for CO₂ over H⁺ reduction were observed for benzimidazol-2-ylidene relative to imidazol-2-ylidene NHC donors.¹⁰ Modification of the annulating moiety has been shown to considerably affect the σ-donating and π-accepting properties of the NHC donor, both of which are significant factors when bonded to a late-transition metal,^{16,17} providing a means of tuning the electronic properties of the complex. In this vein, we have synthesized Pd pincer complexes with further extended π systems attached to the NHC moiety, namely, phenanthro- and pyreno-annulated NHCs, to investigate their relative performance as CO₂ reduction electrocatalysts.^{17,18} Here we demonstrate that these complexes are capable of reducing CO₂ to CO and have additional redox activity, which enables increased electron donation and activation of CO₂.

RESULTS AND DISCUSSION

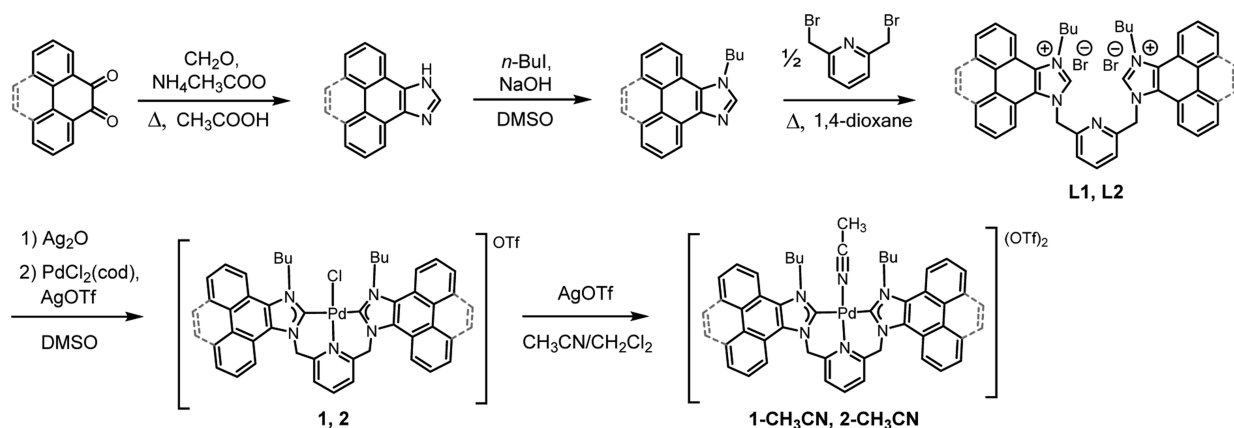
Synthesis and Structure. The proligands were synthesized by condensation of phenanthrene-9,10-dione or pyrene-4,5-dione with formaldehyde and ammonium acetate in acetic acid to yield the polyannulated imidazole, followed by alkylation

with 1-iodobutane and then the addition of 2 equiv to 2,6-bis(bromomethyl)pyridine, yielding the dibromide salt. Coordination to palladium was achieved via transmetalation from a silver carbene intermediate, where the proligand was reacted with 1 equiv of silver(I) oxide in the presence of 3 Å molecular sieves in DMSO and then with equivalents of PdCl₂(cod) and silver triflate once silver(I) oxide had reacted, yielding the [Pd(L)Cl]OTf complexes **1** and **2** in 46–66% isolated yields (Scheme 2). Purification can be achieved either by repeated washes with small aliquots of methanol or by column chromatography using a *N,N*-dimethylformamide (DMF)/CH₃CN/KNO₃(aq) solvent mixture as the eluent. Once synthesized, these complexes were functionalized by halide abstraction using an excess of silver triflate in the presence of a coordinating neutral ligand, in this case acetonitrile, yielding **1-CH₃CN** and **2-CH₃CN** in 66–80% yields.



The complexes were characterized by mass spectrometry (MS), ¹H NMR, and attenuated total reflectance Fourier transform infrared (ATR-FTIR) spectroscopy, with the IR spectra indicating the presence of the bound acetonitrilo ligand for **1-CH₃CN** and **2-CH₃CN** (Figures S7–S12). Microanalysis of **2** yielded inconsistent results. Over four analyses, % N and % H were consistent and within the acceptable range, but % C was consistently 2.7–3.0% below calculated amounts. Microanalysis of the derivative product **2-CH₃CN** matched the predicted % N, % H, and % S but was also 2.6–2.7% below calculated amounts for % C, which cannot be accounted for by the presence of unreacted starting materials or silver carbene intermediates. Incomplete combustion of electropositive complexes with M–C bonds has been observed previously and attributed to carbide formation.^{19–21}

Scheme 2. Synthetic Route to **1**, **2**, **1-CH₃CN**, and **2-CH₃CN**



Both **1** and **2** have low solubility in many organic solvents other than DMF and DMSO, presumably because of intermolecular π -stacking interactions. The acetonitrile complexes **1**-CH₃CN and **2**-CH₃CN have improved, but still limited, solubility in solvents such as acetonitrile, acetone, and dichloromethane. Additionally, both proligands are highly fluorescent under UV irradiation, whereas the palladium complexes are nonemissive, providing a convenient means to detect impurities. The absorption spectrum of **2** shows some absorption at the red end of the spectrum, which could be relevant for photocatalytic applications (Figure S13).

X-ray-quality crystals of **1** were grown by the slow diffusion of diethyl ether into a saturated DMF/CH₃CN solution. Interestingly, syntheses of **1** with [BF₄][−] as the counterion instead of [OTf][−] resulted in the growth of modulated crystals, which contained a periodically expanding and contracting unit cell, requiring an unusual and complicated solution and refinement process.²² Despite repeated attempts under a variety of conditions, X-ray-quality crystals of **2** could not be grown with either tetrafluoroborate or triflate counterions; fine powders were obtained in all cases.

The solid-state structure of **1** (Figure 1) revealed a Pd–pyridyl bond length of 2.048 Å, a Pd–Cl bond length of 2.295

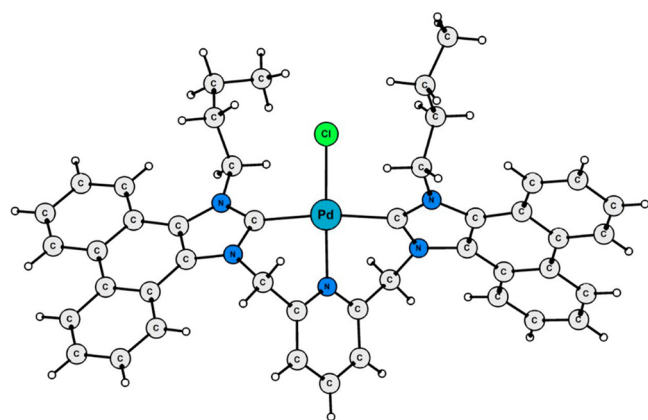


Figure 1. Solid-state structure of **1**. The triflate anion and acetonitrile within the unit cell are omitted.

Å, an average Pd–NHC bond length of 2.038 Å, and a bite angle of 172.0° for the pincer ligand, all of which are comparable to similar complexes with other NHC groups, although the Pd–pyridyl length is approximately 0.02 Å shorter than that in analogous imidazol-2-ylidene and benzimidazol-2-ylidene complexes.^{23–29} This may be due to increased π -back-bonding into the π -acidic pyridyl moiety because the phenanthro-annulated NHC has been shown to have increased π charge density at the carbene center compared with benz-annulated imidazol-2-ylidenes.¹⁷ In general, there is an increasing degree of aromaticity in the imidazol-2-ylidene moiety as the size of the annulated π -system increases, as seen by a downfield shift for the adjacent methylenic protons in the ¹H NMR spectra due to increased ring current, from 5.64 ppm for the bridging methylenic protons in the nonannulated species to 6.04, 6.63, and 6.80 ppm for benz-, phenanthro-, and pyreno-annulated species, respectively.

The NHC moieties are twisted out-of-plane by approximately 45°, comparable to the value in similar lutidine-linked bis-NHC Pd complexes, limiting π stacking in solution and enabling solubility in a few polar aprotic solvents. Within the

unit cell, the phenanthrene moieties of neighboring molecules are aligned with an interplanar distance of 3.4–3.8 Å, which is consistent with the presence of a weak π -stacking interaction.

Electrochemical Characterization under N₂ and CO₂. Complexes **1** and **2** were electrochemically characterized by cyclic and square-wave voltammetry under both N₂ and CO₂ atmospheres, revealing two prominent irreversible reduction waves followed by a larger reduction feature that displays some reversibility for **1** at scan rates above 1 V/s and is reversible for **2**. The irreversible waves were tested for reversibility by immediate postreduction oxidation, but none was detected. The peak potentials for these waves were determined by square-wave voltammetry and are reported in Table 1 and

Table 1. Peak Potentials versus Ferrocene^{0/+} for **1** and **2**^a

complex	$E_{\text{pc}1}$ (V)	$E_{\text{pc}2}$ (V)	$E_{\text{pc}3}$ (V)	$E_{\text{pc}4}$ (V)	$E_{\text{pc}5}$ (V)
1	−1.77	−2.18	−2.49	−2.83 ^b	−2.96
2	−1.74	−2.20 ^b	−2.30 ^b	−2.56 (rev)	

^aRecorded from square-wave voltammograms at 25 Hz for 2 mM solutions in 0.1 M [*n*-Bu₄N]PF₆/DMF under N₂ using a glassy carbon working electrode. ^bPeak potentials determined by deconvolution.

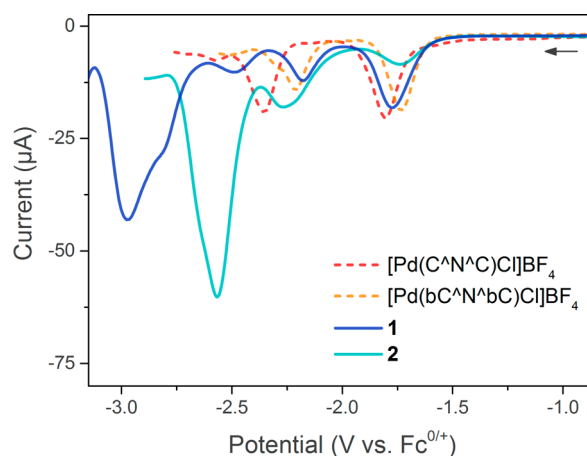


Figure 2. Overlaid square-wave voltammograms of [Pd(C^AN^C)Cl]BF₄, [Pd(bC^AN^bC)Cl]BF₄, **1**, and **2** at 25 Hz.

Figure 2. The first two reduction events were found to occur at potentials very similar to the reduction of [Pd(bC^AN^bC)Cl]BF₄, indicating that the trend of lower reduction potentials with increasing size of the annulated π system did not extend beyond [Pd(bC^AN^bC)Cl]BF₄. The incorporation of phenanthrene and pyrene moieties does, however, lead to new reduction features at approximately −2.92 and −2.57 V for **1** and **2**, respectively, which can be assigned as one-electron reductions of the two polyaromatic moieties present in each complex because the peak current is twice that of the first reduction event in both cases (Figure 3).

At the peak potential of the first reduction event in **1**, a smaller current enhancement in the presence of CO₂ is observed, compared to the current enhancements with [Pd(C^AN^C)Cl]BF₄ and [Pd(bC^AN^bC)Cl]BF₄, and **2** showed no current enhancement at all. This may be due to greater stabilization of the additional charge due to the presence of extended π systems. A large current enhancement was observed for each complex upon transfer of the second

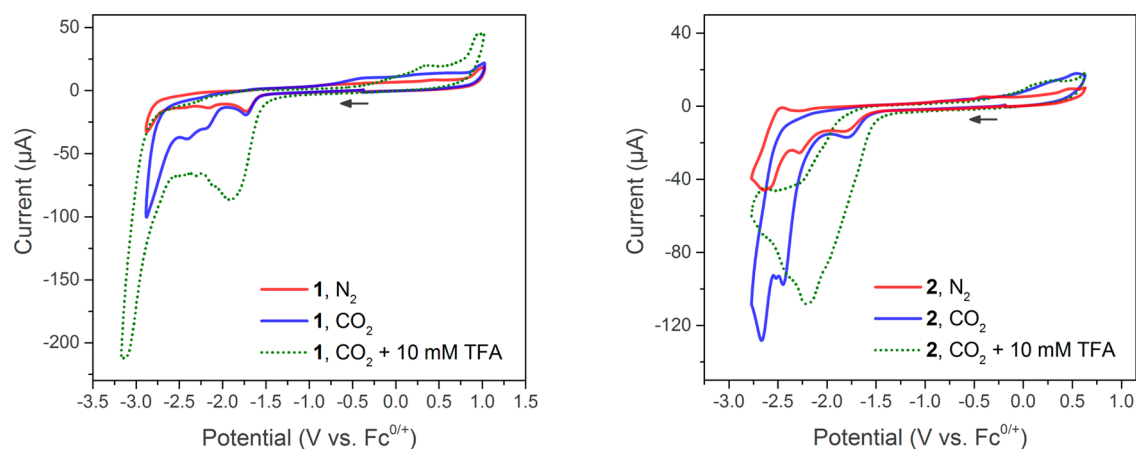


Figure 3. Cyclic voltammograms of **1** (left) and **2** (right) at 100 mV/s under N₂ and CO₂.

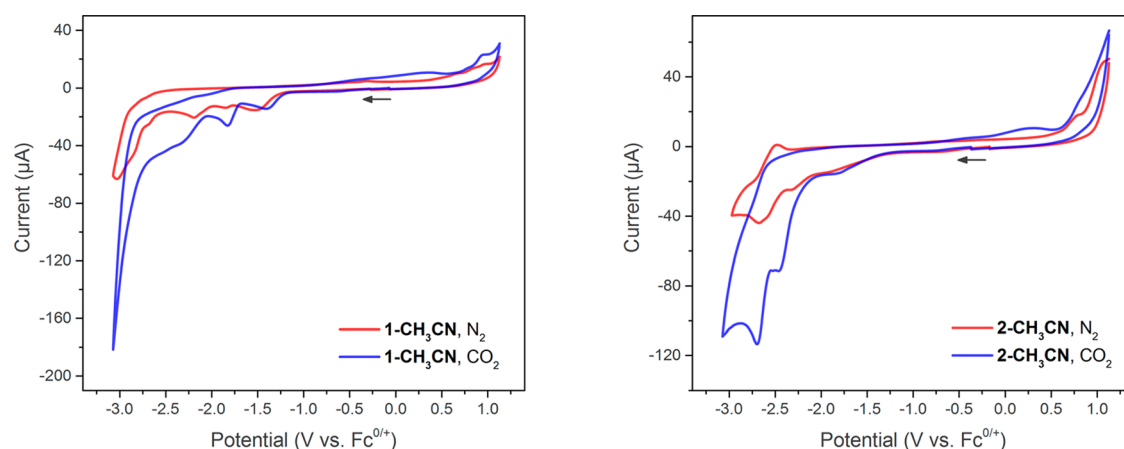


Figure 4. Cyclic voltammograms of **1-CH₃CN** (left) and **2-CH₃CN** (right) at 100 mV/s under N₂ and CO₂.

electron, indicative of chemical reactivity between the reduced complex and CO₂. A further current enhancement was observed upon reduction of the polyaromatic NHC groups, as well as a loss of electrochemical reversibility. This behavior is consistent with an increased degree of CO₂ activation due to increased electron donation from the reduced NHC groups.

In addition, because of the size of the π systems in these molecules, especially **2**, it is conceivable that their electrochemical response could deviate from normal solution behavior because of π interactions between the graphitic surface of the glassy carbon electrode and the complexes. Thus, electrochemical experiments were also performed with a platinum electrode, and these revealed the same characteristics and broad waves as those with glassy carbon. In addition, with either platinum or carbon electrodes and for both complexes, the peak current increased linearly with the square root of the scan rate, indicating freely diffusing species in solution according to the Randles–Sevcik equation.¹² Thus, the relative broadness of the reduction waves, especially evident with **2**, is attributed solely to slower diffusion rates due to the increased size of the molecules as well as some aggregation in solution.

To provide further support for this, ¹H NMR diffusion-ordered spectroscopy (DOSY) experiments were performed to compare the relative diffusion rates of [Pd(bC^NbC)Cl]BF₄, **1**, and **2** in DMSO-*d*₆ because each of these complexes has characteristic, nonoverlapping resonances for the diastereotopic protons of the methylene groups linking the pyridyl rings to the

imidazol-2-ylidenes. These experiments gave diffusion rates of 1.6×10^{-6} cm²/s for [Pd(bC^NbC)Cl]BF₄, 1.3×10^{-6} cm²/s for **1**, and 1.1×10^{-6} cm²/s for **2** in DMSO-*d*₆ (Figures S15 and S16). By a comparison of the conservative estimates of the hydrodynamic radii based on the geometry-optimized DFT structures, decreases in the diffusion rate of 18% from [Pd(bC^NbC)Cl]BF₄ to **1** and then 8% from **1** to **2** are predicted according to the Stokes–Einstein equation.¹² Decreases of 20% and then 14%, respectively, are observed, with this unaccounted-for decrease attributable to π -aggregation interactions, especially in the case of **2**. This is also consistent with the broadness of ¹H NMR resonances for **1** and especially **2**, most prominent at high concentrations, in the high-viscosity NMR solvent DMSO-*d*₆.

The electrochemistry of the dicationic solvento complexes **1-CH₃CN** and **2-CH₃CN** was also analyzed (Figure 4), revealing in both cases an anodic shift in the peak potential of the first cathodic wave, by +0.34 and +0.36 V, respectively, relative to the chloro complexes **1** and **2** (Table 2). As observed previously with related complexes,¹⁰ the dicationic species were able to scavenge trace chloride ions in solution to replace the labile solvento ligand. The addition of tetrabutylammonium chloride to a solution of **1-CH₃CN** led to loss of the cathodic wave at -1.43 V and growth at -1.77 V, matching the electrochemical features of **1**. The addition of tetraoctylammonium bromide to a solution of **1-CH₃CN** led to loss of the cathodic wave at -1.43 V and growth of a new wave at -1.61

Table 2. Peak Potentials versus Ferrocene^{0/+} of the First Cathodic Wave for 1-CH₃CN and 2-CH₃CN Compared to Those of 1 and 2^a

complex	E_{pc1} (V)	$\Delta(E_{\text{pc1}})$ (V)
1	-1.77	
1-CH ₃ CN	-1.43	+0.34
2	-1.76	
2-CH ₃ CN	-1.40	+0.36

^aRecorded from square-wave voltammograms at 25 Hz for 2 mM solutions in 0.1 M [*n*-Bu₄N]PF₆/DMF under N₂ using a glassy carbon working electrode.

V, attributed to a bromo species. The reduction waves at -2.18 V and between -2.83 and -2.96 V are unchanged relative to **1** for both 1-CH₃CN and 1-Br, and the wave at -2.49 V is no longer present (or cathodically shifted). Thus, the potential of the first electron transfer to the complex as well as the third reduction peak in **1** is found to be sensitive to the ligand in the fourth coordination site.

Electrochemical Effects of Stabilizing Cations. Electrochemical characterization of **1** was also carried out in the presence of Mg²⁺ through the addition of 25 mM Mg(ClO₄)₂. Previous investigations have shown that the presence of alkali- and alkali-earth-metal cations can assist in CO₂ reduction by stabilizing the charge buildup on the oxygen atoms of partially activated CO₂.^{10,30–32} In addition to this general CO₂-stabilizing effect, the presence of coordinating cations may be particularly beneficial for electrocatalysts with a pincer motif, where an initial loss of the ligand in the fourth coordination site, often a halide, upon reduction is required for catalytic turnover. For example, it has been shown that palladium triphosphine pincer complexes require a labile solvento ligand in the fourth coordination site for CO₂ reduction activity. Similarly, although there is CO₂ reduction activity with a halide ligand present for lutidine-linked bis-NHC Pd pincer complexes, the performance is improved when the halide is replaced by a solvento ligand.^{7,10} Thus, the presence of more strongly interacting cations in solution may have a dual function by also helping to abstract and/or passivate coordinating anions. Both of these effects can be inferred from a comparison of the cyclic voltammograms of **1** taken under N₂ and CO₂ and with/without Mg²⁺ ions present (Figure 5). Without any CO₂ in solution, the presence of Mg²⁺ ions led to increased current at the second reduction wave, a peak that likely results from the reduction of an electrogenerated species with the chloro ligand dissociated. This assignment is also supported by cyclic voltammograms taken at high scan rates (1–5 V/s), where the second reduction wave diminishes as the scan rate increases (attributed to a chloro-dissociated species), and the third wave at -2.49 V becomes more prominent (attributed to a chloro-bound species). With CO₂ but no proton source in solution, an attenuated current enhancement is observed with Mg²⁺, which can be explained by its stabilizing ability. With a proton source present, the activated CO₂ can be protonated and reduced.

DFT Modeling and Investigations. To gain greater insight into these complexes, DFT calculations were carried out to (1) give optimized solution-state structures of the unreduced and one-, two-, and three-electron-reduced species, (2) determine an approximate degree of activation for CO₂ bound to the reduced species, and (3) calculate the energetics

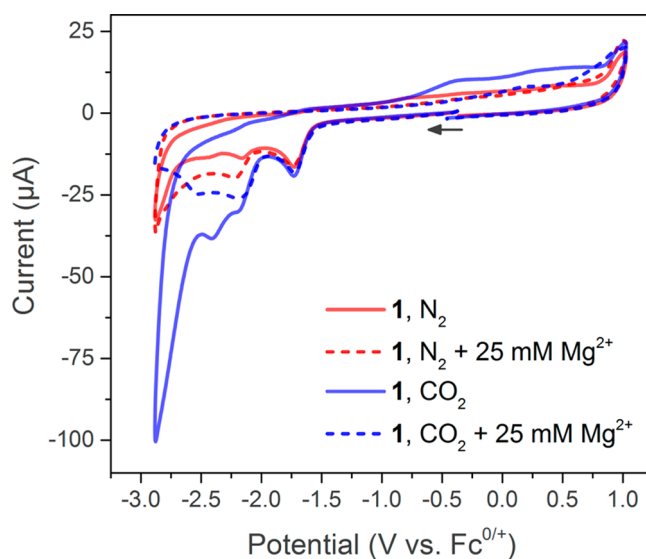


Figure 5. Overlaid cyclic voltammograms of **1** at 100 mV/s under N₂ and CO₂ with and without 25 mM Mg(ClO₄)₂ present.

and activation of CO₂ as it approaches a reduced polyaromatic complex.

A molecular orbital (MO) analysis of DFT-1 and DFT-2 shows a smaller highest occupied molecular orbital (HOMO)/lowest unoccupied molecular orbital (LUMO) gap ($\Delta_{\text{HOMO-LUMO}} = 6.96$ and 6.45 eV, respectively) for the polyaromatic species compared to those of [Pd(C[^]N[^]C)Cl]⁺ ($\Delta_{\text{HOMO-LUMO}} = 8.58$ eV) and [Pd(bC[^]N[^]bC)Cl]⁺ ($\Delta_{\text{HOMO-LUMO}} = 8.42$ eV). There are also additional lower-lying unoccupied MOs available in DFT-1 and DFT-2. Additionally, the polyannulated NHCs were found to be stronger electron donors than analogous (benz)imidazol-2-ylidenes, yielding atomic charges of +0.176 and +0.175 on palladium for DFT-1 and DFT-2 compared to +0.234 and +0.250 for [Pd(C[^]N[^]C)Cl]⁺ and [Pd(bC[^]N[^]bC)Cl]⁺, respectively, based on natural bond orbital (NBO) analyses. In both model systems, the LUMO is localized on the lutidine linker and contains some Pd d_{xz} character (Figure 6). At higher energies than that of the LUMO (approximately +0.75 eV) are a cluster of distinct MOs at very similar energies, providing information about where added electrons may reside on the reduced complexes. Within this cluster, there is an orbital with primarily Pd d_{x²-y²} character and two orbitals with primarily phenanthrene/pyrene character (Figure 6), showing that the polyaromatic NHC ligands can potentially act as electron reservoirs, providing additional redox activity to the pincer proligand. Each of these orbitals are localized in distinct and complementary areas of the molecule, providing potentially good charge diffusion and stabilization when populated.

The relative energies of these orbitals and the order of their population as electrons are added to the system will be perturbed as additional charge is added, especially when there are accompanying geometry changes in the complex. Thus, geometry-optimized structures were calculated as additional electrons were added to the system.



Figure 6. Calculated geometries of low-lying unoccupied MOs for **DFT-2**. LUMO+2 is similar in energy and geometry to LUMO+1 but also contains some pyridyl character.

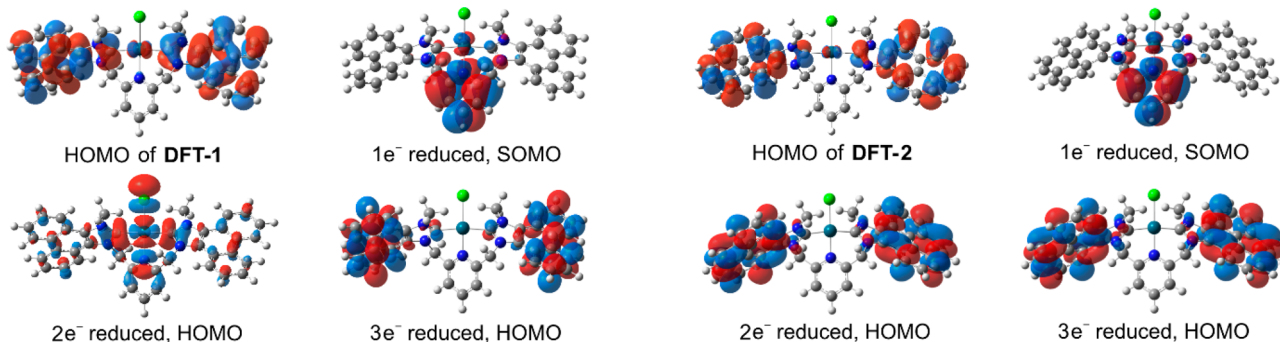
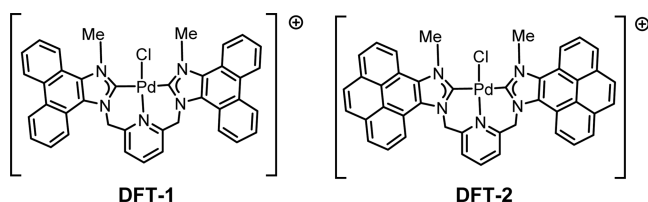


Figure 7. HOMO and SOMO geometries of lowest-energy geometry-optimized structures of reduced species of **DFT-1** and **DFT-2** as pristine, nonhalide-dissociated species.



The first electron added to each of **DFT-1** and **DFT-2** was found to be localized on the pyridyl group, with some Pd and NHC character, and resulted in contraction of the Pd–N bond (from approximately 2.05 to 2.01 Å) and lengthening of the Pd–Cl bond (from approximately 2.30 to 2.38 Å), as well as the lengthening and contraction of bonds within the pyridyl group toward more distinct single bond/double bond character, intermediate to dihydropyridine (Figure 7). The weakening of the Pd–Cl bond is pertinent for catalysis, where displacement of the ligand is necessary. Calculations of the free energy of chloro dissociation were performed on **DFT-1**, **DFT-2**, and a model complex of $[\text{Pd}(\text{C}^{\wedge}\text{N}^{\wedge}\text{C}_{\text{R}=\text{Me}})\text{Cl}]^{\oplus}$, yielding similar results of $+42 \pm 1$ kcal/mol for the nonreduced species and -1 ± 1 kcal/mol for the one-electron-reduced species. The dissociation energies were found to correlate with the basicity of the ligand, where bromo, trifluoroacetate, and trifluoroethanolate have free energies of dissociation of -4 , -11 , and $+8$ kcal/mol, respectively, from the one-electron-reduced species of $[\text{Pd}(\text{C}^{\wedge}\text{N}^{\wedge}\text{C}_{\text{R}=\text{Me}})\text{X}]^{\oplus}$.

The second electron can be added in either a spin-aligned (singlet) or antialigned (triplet) manner. Both configurations were tested and found to be almost identical in energy, with the singlet state being marginally more stable for **DFT-1** and the triplet state slightly more stable for **DFT-2** (by 1–3 kcal/mol). In the triplet state, the electron is localized on the polyaromatic moieties, with the singly occupied molecular orbital (SOMO) in **DFT-2** being 0.42 eV lower in energy because of more extensive π conjugation. In the singlet state, the additional electron is localized across the palladium, NHC, and pyridyl groups, resulting in a further lengthening of the Pd–Cl bond to

2.41 Å. At this point, the chloride has only a small energy barrier to dissociation, which is calculated to be exergonic by approximately 50 kcal/mol. Dissociation of the halide lowers the energy of the empty $d_{x^2-y^2}$ orbital below that of the polyaromatic moieties.

The third electron added to the system for both complexes, even for halide-dissociated species, is localized on the polyaromatic moieties. The LUMO is also phenanthro- or pyrene-localized, which is consistent with the experimental results showing multielectron transfer at the most negative reduction potentials. The characteristics of the modeled reduced species are consistent with the electrochemical data and provide additional insight, suggesting stability of the Pd–NHC bonds even in highly reduced species, weakening of the halide bond by the first two pyridyl/palladium-centered electron transfers, and additional redox activity on the phenanthrene and pyrene moieties upon transfer of three and four electrons.

Another redox-active annulated NHC ligand, naphthoquinoneimidazol-2-ylidene, has been previously reported, showing reversible reduction/oxidation in $\text{Ir}(\text{L})(\text{CO})_2\text{Cl}$ at -1.08 V, a much less negative potential than pyrene (-2.54 V) or phenanthrene (-2.82 V),^{33–35} where reduction of the redox-active group switched the NHC to a more electron-donating state.³⁶ A similar effect would be expected upon reduction of the polyaromatic groups fused to the NHC, providing additional electron donation to a bound CO_2 molecule. For this reason, calculations of the degree of CO_2 activation as a function of the degree of reduction of the complex were investigated and compared to those of other known electrocatalysts. The bond angle of the bound CO_2 at the energy minimum of the reaction coordinate was used as a convenient quantity to represent this, although analysis of the bonding energy along the whole reaction coordinate is required for strict comparisons. These bond angles are dependent on the chosen computational parameters such as the functional and basis set

and are best interpreted as relative assessments of CO₂ activation.

The results of these calculations show an increase in the degree of CO₂ activation by species with reduced polyaromatic moieties, from a bond angle of approximately 128° in two-

Table 3. Calculated Degree of CO₂ Activation When Bound to Reduced Complexes

complex	degree of reduction	CO ₂ bond angle (deg)
DFT-1	2e ⁻	127.6
	3e ⁻	125.8
	4e ⁻	123.8
DFT-2	2e ⁻	128.2
	3e ⁻	127.9
	4e ⁻	123.9

electron-reduced species to 124° in four-electron-reduced species (Table 3). A comparison of the degree of CO₂ activation as determined by the bond angle, when modeled as bound to an active electrocatalyst species, to the proton sources used in CO₂ reduction with the particular electrocatalyst shows a correlation between the degree of activation and pK_a of the proton source required; highly activated CO₂ can be

Table 4. Correlation between the Calculated Degree of CO₂ Activation at the Bonding Potential Energy Minimum and Required Proton Source^{6,7,10,13}

reduced complex	CO ₂ bond angle (deg)	proton source
Re(bpy)(CO) ₃ ⁻	122.5	adventitious H's, H ₂ O
Mn(bpy)(CO) ₃ ⁻	123.7	TFE, methanol, water
Pd(triphos) ⁰	130.0	HBF ₄ , H ₃ PO ₄
Pd(C [^] N [^] C) ⁰	128.0	TFA

protonated by weak acids, and weak acids lead to less undesired H⁺ reduction in CO₂ electroreduction experiments (Table 4). For example, Mn(bpy)(CO)₃(X) requires the use of weak acids like 2,2,2-trifluoroethanol (TFE; pK_a = 23.5 in DMSO¹⁵) to reduce CO₂, whereas reduction using Re(bpy)(CO)₃(X) can proceed without an added proton source because of the difference in the CO₂ activation capability, calculated to bond angles of 123.7° and 122.5° at their potential energy minima, respectively. Thus, it is reasonable that four-electron-reduced species of 1 and 2 may be able to reduce CO₂ in the presence of a weak acid, such as TFE. Accordingly, cyclic voltammograms of 2 and 2-CH₃CN were taken under CO₂, with the addition of TFE resulting in increased current at the wave attributed to reduction of the pyrene moieties (Figure S17), consistent with these theoretical results.

The optimized structures for the highly reduced CO₂-bound species of DFT-1 and DFT-2 were chemically reasonable with square-planar geometry, conventional Pd–L bond lengths, and CO₂ occupying the fourth coordination site. Conversely, optimizations of simpler cationic complexes such as [Pd(C[^]N[^]C)]⁺ and [Pd(bc[^]N[^]bc)]⁺ with three and four electrons added result in distortions toward a tetrahedral geometry, loss of planarity in the pyridyl moiety, and loss of symmetry in pincer coordination. An NBO charge analysis of the optimized structures revealed increased electron density on the NHC moieties relative to the unreduced complex for the three- and four-electron-reduced cases, indicating charge storage. In the four-electron-reduced case, the additional charge

is localized on the pyridyl group, bound CO₂, and metal center; in the three-electron-reduced case, most of the additional charge is located on the periphery of the polyaromatic groups; in the four-electron-reduced case, most of the additional charge is localized on the pyridyl group and metal center, as well.

Last, the thermodynamics of CO₂ coordination to one- and two-electron-reduced DFT-1 was modeled as a function of the distance from the metal center. Compared to [Pd(C[^]N[^]C)-Cl]⁺, the singly reduced species has a slightly more exergonic

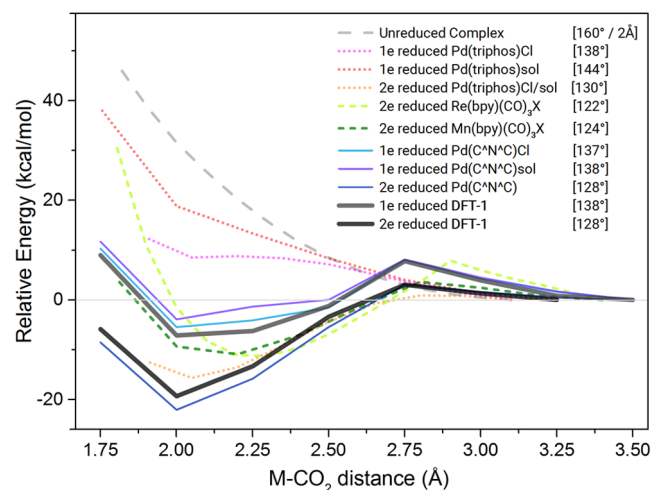


Figure 8. DFT-calculated energetics for the activation of CO₂ as it approaches a reduced metal complex. Bond angles of CO₂ are given at the energy minimum, unless otherwise stated.

interaction, and the doubly reduced species is almost equivalent (Figure 8). Because of the computational expense, only the one- and two-electron-reduced species of DFT-1 were modeled in this way, with only the optimized structures at the energy minima calculated for three- and four-electron-reduced DFT-1 and DFT-2 (see above).

Controlled Potential Electrolysis (CPE). To survey the relative performance of the complexes, CPE experiments were performed at a variety of potentials with CO₂-sparged 2 mM solutions in 0.1 M [*n*-Bu₄N]PF₆/DMF with 10 mM TFA present, unless otherwise specified. The headspace gas was then sampled and analyzed by gas chromatography to quantify the CO and H₂ produced.

Electrolysis at the first reduction potential of 1 led to 18% CO in the gas produced (Table 5). This ratio decreased to 12% at the second reduction potential and then increased to 20% at

Table 5. CPE Results for 1^a

solution	potential (V)	charge passed (C)	ratio of CO produced (%)	FE CO (%)	FE H ₂ (%)
1	-2.02	3.7	18	17	79
1	-2.32	3.7	12	10	68
1	-2.97	3.8	20	15	61
1 + Mg ²⁺	-2.02	3.0	27	26	70
1 + Mg ²⁺	-2.32	3.7	14	11	65
1 + Mg ²⁺	-2.77	4.1	16	14	74
1 ^b	-2.02	68	28	27	69

^aPerformed with a 2 mM solution in 10 mL of 0.1 M [*n*-Bu₄N]PF₆/DMF under CO₂ using a glassy carbon rod working electrode. Potentials versus ferrocene^{0/+}. 25 mM Mg(ClO₄)₂ used, where applicable. ^bA concentration of 1.6 mM 1 was used.

more extreme potentials, where the phenanthrene moieties could be reduced, even though the overpotential for H⁺ reduction at the electrode is very high. The addition of Mg²⁺ improved the selectivity for CO₂ reduction during electrolysis at the first reduction potential, but selectivity at more negative potentials was either comparable or slightly worse.

A longer experiment was also performed where 68 C was passed at −2.02 V and the headspace gas was monitored over six intervals. The ratio of CO produced was consistently between 29 and 32% over the first 56 C and 23% over the last 12 C, representing 5.5 turnovers of CO₂ reduction to produce CO. Cyclic voltammograms taken throughout the experiment retain characteristic features of the complex (Figure S14). Additional TFA was added at intervals of approximately 8 C to maintain its concentration between 2 and 10 mM. The higher efficiency for CO production observed in this longer experiment is attributed to the smaller average concentration of acid present as well as achievement of a steady-state concentration of the active, reduced species. The shorter experiments serve to screen the relative performance at different reduction potentials.

Table 6. CPE Results for 2^a

solution	potential (V)	charge passed (C)	ratio of CO produced (%)	FE CO (%)	FE H ₂ (%)
2	−1.97	3.8	12	12	88
2	−2.32	3.5	7	6	87
2 + Mg ²⁺	−2.02	4.2	11	11	89
2 + Mg ²⁺	−2.32	4.0	12	12	86
2 + Mg ²⁺	−2.62	4.0	13	10	67
2 + 200 mM TFE	−2.77	1.5 ^b	87	33	5

^aPerformed with a 2 mM solution in 10 mL of 0.1 M [*n*-Bu₄N]PF₆/DMF under CO₂ using a glassy carbon rod working electrode. Potentials versus ferrocene^{0/+}. 25 mM Mg(ClO₄)₂ used, where applicable. ^bThe current diminished very quickly as the film formed on the electrode. A potential step to +0.7 V removes the film and recovers a moderate current, which quickly diminishes at −2.77 V.

Electrolysis of 2 yielded similar results, with 12% CO produced at the first reduction potential and a decrease to 7% at the second reduction potential (Table 6). The addition of Mg²⁺ did not result in the same increase in selectivity at the first reduction potential observed with 1, although there was a small improvement during electrolysis at the second and third reduction potentials. Because of the more accessible potential for reduction into the redox-active pyrenoimidazol-2-ylidenes and the effect this could have on the degree of CO₂ activation, electrolysis was attempted at −2.77 V using 200 mM TFE as the proton source. This resulted in selective but short-lived CO₂ reduction, where the current diminished within approximately 15 s of electrolysis. After electrolysis, it was observed that a dark film had deposited on the working electrode. A potential step to +0.7 V removed the film and recovered the initial current, which quickly diminished again upon reduction at −2.77 V. This process was repeated several times and the headspace gas then sampled, revealing 87% CO in the gas produced, which is consistent with greater CO₂ activation resulting from reduction of the high-energy redox-active pyrene moieties. Given that the formation of this film with resulting current deterioration is not observed at these potentials using TFA as the acid source, it may be due to the

formation of an insoluble species by chemical reaction with TFE or its conjugate base.

Electrolysis with 1-CH₃CN revealed an initial ratio of 25% CO produced at −1.67 V, which is an improvement over 17% with the analogous [Pd(C^{^N}^C)(CH₃CN)]²⁺ species.¹⁰ This selectivity also seems to be short-lived, however, because the characteristic electrochemical features for the solvento complex were diminished after the first electrolysis experiment, which may be due to coordination of the generated trifluoroacetate anions. Subsequent experiments showed low selectivities for CO₂ reduction regardless of the potential applied and whether or not Mg²⁺ was added (Table 7). This is in contrast to 1 and also to the simpler complex [Pd(C^{^N}^C)(CH₃CN)]²⁺, which

Table 7. CPE Results for 1-CH₃CN^a

solution	potential (V)	charge passed (C)	ratio of CO produced (%)	FE CO (%)	FE H ₂ (%)
1-CH ₃ CN	−1.67	3.5	25	24	72
1-CH ₃ CN ^b	−1.97	3.5	14	12	78
1-CH ₃ CN	−2.32	3.5	5	4	75
1-CH ₃ CN	−1.67	3.1	5	5	94
1-CH ₃ CN + Mg ²⁺	−1.62	3.5	7	7	90
1-CH ₃ CN + Mg ²⁺	−1.97	3.8	7	7	87
1-CH ₃ CN + Mg ²⁺	−2.17	3.8	6	6	85
1-CH ₃ CN + Mg ²⁺	−2.32	3.8	2	2	80

^aPerformed in sequence from the top to bottom row with a 2 mM solution in 10 mL of 0.1 M [*n*-Bu₄N]PF₆/DMF under CO₂ using a glassy carbon rod working electrode. Potentials versus ferrocene^{0/+}. 25 mM Mg(ClO₄)₂ used, where applicable. ^bThe distinctive electrochemical feature for the acetonitrile complex diminished after CPE at −1.67 V.

maintained selectivity for CO₂ throughout of 6 times the charge transfer.¹⁰

Because of deactivation of 1-CH₃CN during electrolysis with TFA as the proton source and given that its first reduction peak is at −1.43 V, with the current onset at approximately −1.31 V, electrolysis was attempted with the strong acid HPF₆ (pK_a ~ 0 in DMSO^{15,37}) as the proton source, given that its conjugate base is the noncoordinating anion [PF₆][−]. Electrolysis at −1.67 and −1.47 V yielded 6% and 5% CO production, respectively,

Table 8. CPE Results for 1-CH₃CN with 10 mM HPF₆^a

solution	potential (V)	charge passed (C)	ratio of CO produced (%)	FE CO (%)	FE H ₂ (%)
1-CH ₃ CN	−1.67	4.1	6	6	89
1-CH ₃ CN	−1.47	3.0	5	5	91
1-CH ₃ CN	−2.32	2.2	3	2	73
1-CH ₃ CN + Mg ²⁺	−1.82	3.0	4	4	97
1-CH ₃ CN + Mg ²⁺	−2.32	3.0	4	3	83

^aPerformed with a 2 mM solution in 10 mL 0.1 M [*n*-Bu₄N]PF₆/DMF under CO₂ using a glassy carbon rod working electrode. Potentials versus ferrocene^{0/+}. 25 mM Mg(ClO₄)₂ used, where applicable.

with H⁺ reduction predominant with this proton source (Table 8). Despite the poor selectivity for CO₂ reduction, the cyclic voltammograms of the complex before and after electrolysis experiments were more consistent, suggesting that inhibition of the complex with the conjugate base of the proton source may be a relevant factor.

Finally, separate electrolysis experiments were carried out with 2-CH₃CN using TFE and TFA as proton sources (Table

Table 9. CPE Results for 2-CH₃CN^a

solution	potential (V)	charge passed (C)	ratio of CO produced (%)	FE CO (%)	FE H ₂ (%)
2-CH ₃ CN + TFE	-2.52	0.5 ^b	100	12	0
2-CH ₃ CN + TFE	-2.72	1.0 ^b	100	14	0
2-CH ₃ CN	-2.07	2.6	4	4	84
2-CH ₃ CN	-2.47	2.5	6	4	73
2-CH ₃ CN + Mg ²⁺	-2.07	3.1	2	1	74
2-CH ₃ CN + Mg ²⁺	-2.47	3.2	12	8	59
2-CH ₃ CN + Mg ²⁺	-2.72	3.2	9	5	49

^aPerformed with a 2 mM solution in 10 mL of 0.1 M [*n*-Bu₄N]PF₆/DMF under CO₂ using a glassy carbon rod working electrode. Potentials versus ferrocene^{0/+}. 500 mM TFE and 25 mM Mg(ClO₄)₂ used, where applicable. ^bThe current diminished quickly as the film formed on the electrode. A potential step to +0.7 V removes the film and recovers a moderate current, which quickly diminishes at these potentials.

9). With TFE, behavior similar to that for 2 was observed, with the formation of a film on the electrode surface and a quickly diminishing current, resulting in the reduction of CO₂ to CO. Again, holding the working electrode at +0.7 V resulted in removal of the film and a temporarily restored current. With TFA, selectivities for CO production were lower than those with 1, 2, or 1-CH₃CN at 4–12%, and a noticeable amount of a dark precipitate was formed. This insoluble black powder was isolated by centrifugation, dried, and analyzed by ATR-FTIR, revealing features similar to those of 2 but with a strong, broad stretch centered at 1854 cm⁻¹ (Figure S15), tentatively assigned to a carbonate or bicarbonate species.

Colorimetric spot tests with chromotropic acid and methylquinaldinium^{38,39} were performed on the solutions after electrolysis to test for the presence of formic acid, formate, or formaldehyde; none of these species were detected. Additionally, two CPE experiments were performed with 2-CH₃CN in acetonitrile, with the resulting solution analyzed by ¹H NMR in CD₃CN with suppression of the acetonitrile solvent signal (1.96 ppm), which is well separated from signals for formate/formic acid (8.0 ppm) and formaldehyde (9.6 ppm). Again, none of these potential reduction products was detected. Finally, two experiments were performed to see if heterogeneous catalysis may be a significant contributor to the production of CO: a mercury drop test was performed with 1 at -2.05 V, revealing no difference in the performance, and after an electrolysis experiment with 1, the working electrode was transferred to a new electrolyte solution with 10 mM TFA but no dissolved complex. The passage of 5 C resulted in a ratio of only 1% CO produced.

CONCLUSION

Phenanthro- and pyreno-annulated bis-NHC Pd pincer complexes 1 and 2 were synthesized and found to have reduction potentials similar to that of [Pd(bC[^]N[^]bC)Cl]⁺. These complexes are able to electrocatalytically reduce CO₂ to CO in the presence of TFA, with 1 having appreciably improved selectivity for CO₂ reduction at the first reduction potential compared to [Pd(C[^]N[^]C)Cl]⁺ and [Pd(bC[^]N[^]bC)-Cl]⁺ and 2 having diminished relative selectivity, showing that electronic modifications to the NHC donors can drastically

affect the reactivity. The solvento complexes 1-CH₃CN and 2-CH₃CN were found to be more quickly deactivated during electrolysis. The addition of polyaromatic groups enabled additional redox activity on the ligand at -2.96 V for 1 and -2.56 V for 2, allowing for increased electron donation from the ligand. The addition of the weak acid TFE results in reactivity with CO₂ at these potentials, but CPEs are short-lived and result in the formation of an insulating and insoluble species on the electrode. These systems were also modeling computationally, providing support for assignments of the redox events, giving a greater understanding of the chemical behavior of the reduced species, and highlighting the importance of anion dissociation energies within the pincer motif. Investigations into the effects of modifying the pyridyl moiety and metal center are currently underway.

EXPERIMENTAL SECTION

General Procedures. Unless otherwise specified, all reactions were performed under nitrogen using standard Schlenk techniques and solvents and reagents were used as received from commercial sources. Magnesium perchlorate (Alfa), 2,2,2-trifluoroethanol (TFE; Aldrich), and trifluoroacetic acid (TFA; Aldrich) were used as received for electrochemical experiments. *N,N*-Dimethylformamide (DMF; EMD Millipore Omnisolv) and distilled acetonitrile (Anachemia Accusolv) were dried and stored over 15% (m/v) 4 Å molecular sieves.^{40,41}

¹H NMR spectra were acquired using Bruker AV300 or AV400 spectrometers with chemical shifts referenced to residual solvent signals. Mass spectra were acquired using a Waters LC-MS electrospray ionization mass spectrometer, except for the acetonitrile complexes, which were acquired using a Waters Micromass LCT electrospray ionization mass spectrometer. IR spectra were collected using a PerkinElmer Frontier FTIR spectrometer with an ATR attachment. Gaseous products were analyzed using an SRI model 8610C gas chromatograph equipped with molecular-sieve columns, dual thermal conductivity and flame ionization detectors, and a methanizer. Crystallographic data were acquired using a Bruker X8 APEX II diffractometer with graphite-monochromated Mo K α radiation.

Electrochemistry. Electrochemical experiments were performed using a Metrohm Autolab PGSTAT12 or Pine AFCBP1 bipotentiostat in an airtight three-electrode cell with a 7 mm² glassy carbon working electrode (Bioanalytical Systems, Inc.), platinum mesh counter electrode, and silver wire pseudoreference electrode in a 0.010 M AgNO₃ acetonitrile solution separated from the bulk solution by a Vycor frit. Experiments were performed under N₂ or CO₂ using 2 mM concentrations of the complexes in 10 mL of an anhydrous electrolyte solution unless otherwise stated. CPE experiments used glassy carbon rod (Alfa Aesar) working electrodes in a two compartment H cell, where the counter electrode compartment was separated from the compartment containing the working and reference electrodes by fritted glass. All glassy carbon electrodes were cleaned by successive polishing with 1, 0.3, and 0.05 μ M alumina paste, followed by rinsing with water, sonication (5 min) in distilled water, and sonication (5 min) in methanol. Electrolyte solutions were 0.10 M triply recrystallized [*n*-Bu₄N]PF₆ in anhydrous DMF and sparged with nitrogen prior to use. For experiments with CO₂, the solution was sparged with CO₂ for 15 min. Decamethylferrocene was added at the end of the electrochemical experiments as an internal standard, showing a reversible redox couple at -404 mV vs Ag/AgNO₃ and -476 mV vs ferrocene/ferrocenium in 0.1 M [*n*-Bu₄N]PF₆/DMF.⁴² Cyclic voltammograms were collected at a scan rate of 100 mV/s and square-wave voltammograms at a frequency of 25 Hz unless otherwise stated.

Computational Methods. DFT calculations were performed using *Gaussian 09* (revision D.01) with the long-range and dispersion-corrected ω B97xD hybrid functional without symmetry constraints.⁴³ Calculations for reduced species were performed using unrestricted, open-shell wave functions. The D95(d) basis set was used for all atoms

except transition metals, which employed the Stuttgart–Dresden–Bonn quasi-relativistic effective-core potential and corresponding correlation-consistent triple- ζ basis set.^{44,45} Calculations were performed with the presence of a solvent reaction field of acetonitrile produced by the conductor-like polarizable continuum model.⁴⁶ Frequency calculations were performed on all geometry-optimized structures to ensure that energy minima were achieved.

Synthesis. The proligand precursor 9,10-phenanthrenequinone (95%) was purchased from Sigma-Aldrich, with the remaining precursors synthesized according to literature procedures: 2,6-bis(bromomethyl)pyridine,⁴⁷ 1*H*-phenanthro[9,10-*d*]imidazole,¹⁷ pyrene-4,5-dione,⁴⁸ and 9*H*-pyreno[4,5-*d*]imidazole.¹⁸

Alkylation of Polyaromatic Imidazoles. **1-Butyl-1*H*-phenanthro[9,10-*d*]imidazole.** The compound was synthesized via a modified literature procedure.¹⁷ Sodium hydroxide (4.40 mmol, 176 mg) was added to a 10 mL solution of 1*H*-phenanthro[9,10-*d*]imidazole (3.99 mmol, 870 mg) in DMSO and stirred for 2 h at room temperature, after which 1-iodobutane (4.5 mmol, 0.51 mL) was added and the solution was heated to 50 °C overnight. Water (15 mL) was added to the solution and extracted with diethyl ether (15 mL \times 4). The organic extracts were washed with water (15 mL \times 2) and then the solvent was removed, yielding a yellow-orange oil (899 mg). The crude product was purified by column chromatography over SiO₂ using acetone as the eluent, collecting the second band. Upon removal of the solvent, the oil crystallized as a yellow-orange solid (813 mg, 74% yield). ¹H NMR (300 MHz, (CD₃)₂CO): δ 0.98 (t, *J* = 7.4 Hz, 3 H), 1.48 (sxt, *J* = 7.5 Hz, 2 H), 2.02 (quin, *J* = 7.5 Hz, 2 H), 4.78 (t, *J* = 7.2 Hz, 2 H), 7.55–7.79 (m, 4 H), 8.12 (s, 1 H), 8.41 (dt, *J* = 8.0 and 0.9 Hz, 1 H), 8.62–8.71 (m, 1 H), 8.81 (dt, *J* = 8.2 and 0.7 Hz, 1 H), 8.93 (dt, *J* = 8.2 and 0.8 Hz, 1 H).

9-Butyl-9*H*-pyreno[4,5-*d*]imidazole. The compound was synthesized via a modified literature procedure.¹⁸ Sodium hydroxide (3.90 mmol, 156 mg) was added to a 12 mL solution of 9*H*-pyreno[4,5-*d*]imidazole (3.55 mmol, 860 mg) in DMSO and stirred for 2 h at room temperature, after which 1-iodobutane (4.0 mmol, 0.45 mL) was added and the solution was heated to 50 °C overnight. Water (15 mL) was added to the solution and extracted with diethyl ether (25 mL \times 5). The organic extracts were washed with water (20 mL \times 2) and dried with MgSO₄, and the solvent was then removed, yielding an orange crystalline powder (589 mg, 56% yield), which was used without further purification. ¹H NMR (300 MHz, (CD₃)₂SO): δ 0.89 (t, *J* = 7.3 Hz, 3 H), 1.38 (sxt, *J* = 7.3 Hz, 2 H), 1.93 (quin, *J* = 7.2 Hz, 2 H), 4.78 (t, *J* = 7.1 Hz, 2 H), 8.07–8.14 (m, 2 H), 8.17 (s, 2 H), 8.19–8.27 (m, 2 H), 8.36 (s, 1 H), 8.57 (d, *J* = 7.6 Hz, 1 H), 8.80 (dt, *J* = 7.5 and 0.6 Hz, 1 H).

Synthesis of Proligands. **phenC[^]N[^]phenC-2*HBr* (L1).** A solution of 1-butyl-1*H*-phenanthro[9,10-*d*]imidazole (2.96 mmol, 813 mg) and 2,6-bis(bromomethyl)pyridine (1.40 mmol, 372 mg) in 20 mL of 1,4-dioxane was heated to reflux for 84 h, during which time an off-white precipitate was formed. The precipitate was collected by centrifugation, washed with diethyl ether (10 mL \times 2), and then dried under vacuum, yielding an off-white powder (732 mg, 64% yield). ¹H NMR (300 MHz, (CD₃)₂SO): δ 0.97 (t, *J* = 7.3 Hz, 6 H), 1.43 (sxt, *J* = 7.3 Hz, 4 H), 1.74 (quin, *J* = 7.4 Hz, 4 H), 4.38 (t, *J* = 7.4 Hz, 4 H), 6.14 (s, 4 H), 7.23 (t, *J* = 7.8 Hz, 2 H), 7.55 (t, *J* = 7.8 Hz, 2 H), 7.66 (d, *J* = 8.4 Hz, 2 H), 7.71–7.85 (m, 6 H), 8.05 (d, *J* = 8.1 Hz, 2 H), 8.20 (t, *J* = 7.8 Hz, 1 H), 8.46 (d, *J* = 8.4 Hz, 2 H), 8.54 (d, *J* = 8.3 Hz, 2 H), 9.47 (s, 2 H). ESI-MS: *m/z* 732.8 ([M – Br]⁺).

pyreC[^]N[^]pyreC-2*HBr* (L2). A solution of 9-butyl-9*H*-pyreno[4,5-*d*]imidazole (1.46 mmol, 436 mg) and 2,6-bis(bromomethyl)pyridine (0.710 mmol, 188 mg) in 15 mL of 1,4-dioxane was heated to reflux for 84 h, during which a light-colored precipitate was formed. The precipitate was collected by centrifugation, washed with diethyl ether (10 mL \times 2), and then dried under vacuum, yielding an off-white powder (411 mg, 67% yield). ¹H NMR (300 MHz, (CD₃)₂SO): δ 0.98 (t, *J* = 7.3 Hz, 6 H), 1.44 (sxt, *J* = 7.4 Hz, 4 H), 1.71 (quin, *J* = 7.4 Hz, 4 H), 4.25 (t, *J* = 7.5 Hz, 4 H), 6.23 (s, 4 H), 7.54 (t, *J* = 7.9 Hz, 2 H), 7.80–8.04 (m, 14 H), 8.20 (dt, *J* = 7.3 and 0.8 Hz, 2 H), 8.29 (t, *J* = 7.8 Hz, 1 H), 9.58 (s, 2 H). ESI-MS: *m/z* 780.9 ([M – Br]⁺).

Synthesis of Halide Complexes. **[Pd(phenC[^]N[^]phenC)Cl]OTf (1).** To a solution of L1 (0.369 mmol, 300 mg) in DMSO (12 mL) was added Ag₂O (0.368 mmol, 85.3 mg) and 3 Å molecular sieves. The reaction vessel was covered in foil and left to stir at 50 °C for 24 h and then left to cool to room temperature. To the resulting mixture was added PdCl₂(cod) (0.369 mmol, 105 mg) and then AgOTf (0.405 mmol, 104 mg). The mixture was left to stir for 48 h, then centrifuged, and filtered through Celite. The solvent was removed under vacuum at 55 °C and the residue taken up in acetonitrile (5 mL). Addition to Et₂O (12 mL) yielded a light-yellow precipitate, which was isolated by centrifugation and washed with Et₂O (5 mL), MeOH (2 mL), and Et₂O (5 mL), yielding the crude product (260 mg). Purification was achieved by successive washes with a minimum of MeOH (4 \times 1 mL), yielding a light-tan powder (160 mg, 46% yield). X-ray-quality crystals were grown by the slow diffusion of Et₂O into a concentrated 1:1 DMF/CH₃CH solution at –30 °C. ¹H NMR (400 MHz, (CD₃)₂SO): δ 0.94 (t, *J* = 7.3 Hz, 6 H), 1.31–1.43 (m, 2 H), 1.55–1.68 (m, 2 H), 1.87–1.99 (m, 2 H), 2.00–2.12 (m, 2 H), 5.24–5.36 (m, 2 H), 5.48–5.63 (m, 2 H), 6.41 (d, *J* = 15.9 Hz, 2 H), 6.90 (d, *J* = 15.4 Hz, 2 H), 7.79–7.95 (m, 8 H), 8.16 (s, 3 H), 8.57 (d, *J* = 8.2 Hz, 2 H), 8.99 (dt, *J* = 8.4 and 0.7 Hz, 2 H), 9.07 (d, *J* = 8.2 Hz, 2 H), 9.08 (d, *J* = 8.2 Hz, 2 H). ESI-MS: *m/z* 792.6 ([M – OTf]⁺). Anal. Calcd for C₄₆H₄₁ClF₃N₃O₃PdS: C, 58.60; H, 4.38; N, 7.43. Found: C, 58.09; H, 4.41; N, 7.19. Averaged results for repeat elemental analysis are shown. For one attempt, the C was within error of the calculated value, but for the other, it was below. This is accounted for by the presence of a small amount (~7%) of bromo species present, as shown by ESI-MS at *m/z* 838 ([M_{Br} – OTf]⁺), as well as some intractable DMSO (3 mol % by NMR), giving calculated values of 58.36% C, 4.38% H, and 7.39% N.

[Pd(pyreC[^]N[^]pyreC)Cl]OTf (2). To a solution of L2 (0.319 mmol, 275 mg) in DMSO (12 mL) was added Ag₂O (0.324 mmol, 75.1 mg) and 3 Å molecular sieves. The reaction vessel was covered in foil, left to stir at 55 °C for 24 h, and then left to cool to room temperature. To the resulting mixture was added PdCl₂(cod) (0.319 mmol, 99.1 mg) and then AgOTf (0.351 mmol, 90.2 mg). The mixture was left to stir for 56 h, then centrifuged, and filtered through Celite. The solvent was removed under vacuum at 60 °C and the dark residue taken up in acetonitrile (5 mL). Addition to Et₂O (10 mL) yielded a yellow-orange precipitate, which was isolated by centrifugation and washed with Et₂O (5 mL), MeOH (4 \times 2 mL), and Et₂O (5 mL), yielding a tan powder (215 mg, 68% yield). The solutes from methanol washes were analyzed by NMR to track the degree of purification. ¹H NMR (400 MHz, (CD₃)₂SO): δ 0.99 (t, *J* = 7.4 Hz, 6 H), 1.39–1.55 (m, 2 H), 1.64–1.79 (m, 2 H), 2.09 (s, 2 H), 2.11–2.24 (m, 2 H), 5.40–5.53 (m, 2 H), 5.64–5.81 (m, 2 H), 6.53 (d, *J* = 15.9 Hz, 1 H), 7.12 (d, *J* = 15.7 Hz, 2 H), 8.18–8.38 (m, 11 H), 8.47 (d, *J* = 7.8 Hz, 2 H), 8.50 (d, *J* = 7.5 Hz, 3 H), 8.88 (d, *J* = 8.4 Hz, 2 H), 9.33 (d, *J* = 8.2 Hz, 2 H). ESI-MS: *m/z* 840.6 ([M – OTf]⁺). Anal. Calcd for C₅₀H₄₁ClF₃N₃O₃PdS: C, 60.61; H, 4.17; N, 7.07. Found: C, 57.76; H, 4.06; N, 7.21.

Synthesis of Acetonitrile Complexes. **[Pd(phenC[^]N[^]phenC)-(CH₃CN)](OTf)₂ (1-CH₃CN).** Complex 1 (0.050 mmol, 47 mg) was taken up in a solvent mixture of 20 mL of 1:1 CH₃CN/CH₂Cl₂, and the light-yellow solution was reacted with AgOTf (0.11 mmol, 27 mg) at room temperature overnight in the dark, forming a fine white precipitate. The precipitate was removed by centrifugation and the solvent removed under reduced pressure, leaving a light-yellow residue, which was taken up in CH₂Cl₂ (3 mL), reprecipitated by the addition of Et₂O, washed with Et₂O (2 \times 3 mL), and then dried under vacuum, yielding an off-white powder (36 mg, 66% yield). ¹H NMR (400 MHz, CD₃CN): δ 0.98 (t, *J* = 7.4 Hz, 6 H), 1.37–1.51 (m, 2 H), 1.59–1.73 (m, 2 H), 1.92–2.07 (m, 4 H), 1.96 (s, 3 H), 5.00 (dt, *J* = 14.9 and 8.1 Hz, 2 H), 5.23 (dt, *J* = 14.9 and 6.2 Hz, 2 H), 6.29 (d, *J* = 15.7 Hz, 2 H), 6.75 (d, *J* = 15.9 Hz, 2 H), 7.81–8.01 (m, 10 H), 8.09 (t, *J* = 8.0 Hz, 1 H), 8.54 (dt, *J* = 8.2 and 0.7 Hz, 2 H), 8.80 (dt, *J* = 8.3 and 0.7 Hz, 2 H), 8.98 (d, *J* = 8.2 Hz, 2 H), 8.99 (d, *J* = 8.2 Hz, 2 H). ESI-MS: *m/z* 377.9 ([M – CH₃CN – 2(OTf)]²⁺), 905.6 ([M – CH₃CN – OTf]⁺).

[Pd(pyreC[^]N[^]pyreC)(CH₃CN)](OTf)₂ (**2-CH₃CN**). Complex **2** (0.082 mmol, 81 mg) was taken up in a solvent mixture of 20 mL of 1:1:0.1 CH₃CN/CH₂Cl₂/DMF. The dark-orange solution was reacted with AgOTf (0.15 mmol, 38 mg) at room temperature for 4 h in the dark, forming a light-yellow precipitate. The precipitate was removed by centrifugation and the solution concentrated to ~1 mL under reduced pressure. Et₂O (5 mL) was added, inducing precipitation of a sticky orange solid, which was collected and triturated with CHCl₃ (2 mL) and washed with Et₂O (2 × 3 mL). The resulting light-orange powder was dissolved in CH₃CN (2 mL) and precipitated by the addition of Et₂O (5 mL). The tan powder was dried under a stream of N₂ and then under vacuum, yielding a tan powder (75 mg, 80% yield). ¹H NMR (400 MHz, CD₃CN): δ 1.05 (t, J = 7.4 Hz, 6 H), 1.48–1.63 (m, 2 H), 1.73–1.85 (m, 2 H), 1.91–2.02 (m, 2 H), 1.96 (s, 3 H), 2.08–2.20 (m, 2 H), 5.10–5.22 (m, 2 H), 5.37–5.49 (m, 2 H), 6.45 (d, J = 15.9 Hz, 2 H), 6.99 (d, J = 15.7 Hz, 2 H), 8.08 (s, 4 H), 8.29–8.39 (m, 7 H), 8.47 (d, J = 7.7 Hz, 2 H), 8.50 (d, J = 7.8 Hz, 2 H), 8.87 (d, J = 8.0 Hz, 2 H), 9.16 (d, J = 8.0 Hz, 2 H). ESI-MS: m/z 402.7 [M – CH₃CN – 2(OTf)]²⁺. Anal. Calcd for C₅₂H₄₃F₆N₆O₄PdS₂: C, 55.15; H, 3.83; N, 7.42; S, 5.60. Found: C, 52.49; H, 3.78; N, 7.40; S, 5.36.

■ ASSOCIATED CONTENT

● Supporting Information

The Supporting Information is available free of charge on the ACS Publications website at DOI: 10.1021/acs.inorgchem.5b01698.

¹H NMR spectra of proligand precursors, proligands, and complexes, ATR-FTIR spectra of complexes, UV–vis spectra of **1** and **2**, cyclic voltammograms, DOSY NMR data, crystallography details, plots of *i*_p vs *ν*^{1/2} for complexes, and DFT calculation sample input (PDF) X-ray crystallographic data in CIF format (CIF)

■ AUTHOR INFORMATION

Corresponding Author

*E-mail: mwolf@chem.ubc.ca. Phone: (604) 822-1702. Fax: (604) 822-2847.

Notes

The authors declare no competing financial interest.

■ ACKNOWLEDGMENTS

This research was supported by the Natural Sciences and Engineering Research Council of Canada (NSERC). WestGrid (www.westgrid.ca) and Compute Canada–Calcul Canada (www.computeCanada.ca) are acknowledged for access to computational resources for DFT calculations. Prof. David Wilkinson is thanked for use of the gas chromatograph. J.A.T. thanks the NSERC for scholarship funding.

■ REFERENCES

- Inglis, J. L.; MacLean, B. J.; Pryce, M. T.; Vos, J. G. *Coord. Chem. Rev.* **2012**, *256*, 2571.
- Costentin, C.; Robert, M.; Savéant, J.-M. *Chem. Soc. Rev.* **2013**, *42*, 2423.
- Appel, A. M.; Bercaw, J. E.; Bocarsly, A. B.; Dobbek, H.; DuBois, D. L.; Dupuis, M.; Ferry, J. G.; Fujita, E.; Hille, R.; Kenis, P. J. A.; Kerfeld, C. A.; Morris, R. H.; Peden, C. H. F.; Portis, A. R.; Ragsdale, S. W.; Rauchfuss, T. B.; Reek, J. N. H.; Seefeldt, L. C.; Thauer, R. K.; Waldrop, G. L. *Chem. Rev.* **2013**, *113*, 6621.
- Mikkelsen, M.; Jørgensen, M.; Krebs, F. C. *Energy Environ. Sci.* **2010**, *3*, 43.
- Slater, S.; Wagenknecht, J. H. *J. Am. Chem. Soc.* **1984**, *106*, 5367.
- Hawecker, J.; Lehn, J.-M.; Ziessel, R. *J. Chem. Soc., Chem. Commun.* **1984**, *984*, 328.

- DuBois, D. L.; Miedaner, A.; Haltiwanger, R. C. *J. Am. Chem. Soc.* **1991**, *113*, 8753.
- DuBois, D. L. *Comments Inorg. Chem.* **1997**, *19*, 307.
- DuBois, D. L.; Miedaner, A. *J. Am. Chem. Soc.* **1987**, *109*, 113.
- Therrien, J. A.; Wolf, M. O.; Patrick, B. O. *Inorg. Chem.* **2014**, *53*, 12962.
- Keith, J. A.; Grice, K. A.; Kubiak, C. P.; Carter, E. A. *J. Am. Chem. Soc.* **2013**, *135*, 15823.
- Bard, A.; Faulkner, L. *Electrochemical Methods: Fundamentals and Applications*; 2nd ed.; John Wiley & Sons Inc.: New York, 2001.
- Smieja, J. M.; Sampson, M. D.; Grice, K. A.; Benson, E. E.; Froehlich, J. D.; Kubiak, C. P. *Inorg. Chem.* **2013**, *52*, 2484.
- Smieja, J. M.; Kubiak, C. P. *Inorg. Chem.* **2010**, *49*, 9283.
- Bordwell, F. G. *Acc. Chem. Res.* **1988**, *21*, 456.
- Díez-González, S.; Nolan, S. P. *Coord. Chem. Rev.* **2007**, *251*, 874.
- Tapu, D.; Owens, C.; VanDerveer, D.; Gwaltney, K. *Organometallics* **2009**, *28*, 270.
- Valdés, H.; Poyatos, M.; Peris, E. *Organometallics* **2014**, *33*, 394.
- Voges, M. H.; Romming, C.; Tilset, M. *Organometallics* **1999**, *18*, 529.
- Ullah, F.; Bajor, G.; Veszprémi, T.; Jones, P. G.; Heinicke, J. W. *Angew. Chem., Int. Ed.* **2007**, *46*, 2697.
- Gardner, B. M.; McMaster, J.; Liddle, S. T. *Dalt. Trans.* **2009**, 6924.
- Bolotina, N. B. *Crystallogr. Rep.* **2007**, *52*, 647–658.
- Nielsen, D. J.; Cavell, K. J.; Skelton, B. W.; White, A. H. *Inorg. Chim. Acta* **2006**, *359*, 1855.
- Andrew, R. E.; Chaplin, A. B. *Dalton Trans.* **2014**, *43*, 1413.
- Nielsen, D. J.; Cavell, K. J.; Skelton, B. W.; White, A. H. *Inorg. Chim. Acta* **2002**, *327*, 116.
- Danopoulos, A. A.; Tulloch, A. A. D.; Winston, S.; Eastham, G.; Hursthouse, M. B. *Dalt. Trans.* **2003**, 1009.
- Gründemann, S.; Albrecht, M.; Loch, J. A.; Faller, J. W.; Crabtree, R. H. *Organometallics* **2001**, *20*, 5485.
- Hahn, F. E.; Jahnke, M. C.; Gomez-Benitez, V.; Morales-Morales, D.; Pape, T. *Organometallics* **2005**, *24*, 6458.
- Allen, F. H. *Acta Crystallogr., Sect. B: Struct. Sci.* **2002**, *58*, 380.
- Gambarotta, S.; Arena, F.; Floriani, C.; Zanazzi, P. F. *J. Am. Chem. Soc.* **1982**, *104*, 5082.
- Schmidt, M. H.; Miskelly, G. M.; Lewis, N. S. *J. Am. Chem. Soc.* **1990**, *112*, 3420.
- Bhugun, I.; Lexa, D.; Savéant, J.-M. *J. Am. Chem. Soc.* **1996**, *118*, 1769.
- Briegleb, G. *Angew. Chem., Int. Ed. Engl.* **1964**, *3*, 617.
- Goodnow, T. T.; Kaifer, A. E. *J. Phys. Chem.* **1990**, *94*, 7682.
- Aranzaes, J. R.; Daniel, M.; Astruc, D. *Can. J. Chem.* **2006**, *84*, 288.
- Rosen, E. L.; Varnado, C. D.; Tennyson, A. G.; Khramov, D. M.; Kamplain, J. W.; Sung, D. H.; Cresswell, P. T.; Lynch, V. M.; Bielawski, C. W. *Organometallics* **2009**, *28*, 6695.
- Kütt, A.; Rodima, T.; Saame, J.; Raamat, E.; Mäemets, V.; Kaljurand, I.; Koppel, I. A.; Garlyauskayte, R. Y.; Yagupolskii, Y. L.; Yagupolskii, L. M.; Bernhardt, E.; Willner, H.; Leito, I. *J. Org. Chem.* **2011**, *76*, 391.
- Feigl, F.; Anger, V. *Spot Tests in Organic Analysis*, 7th ed.; Elsevier Science: Amsterdam, The Netherlands, 1966.
- Arana, C.; Keshavarz, M.; Potts, K. T.; Abruña, H. D. *Inorg. Chim. Acta* **1994**, *225*, 285.
- Burfield, D. R.; Smithers, R. H. *J. Org. Chem.* **1978**, *43*, 3966.
- Williams, D. B. G.; Lawton, M. J. *J. Org. Chem.* **2010**, *75*, 8351.
- Noviandri, I.; Brown, K. N.; Fleming, D. S.; Gulyas, P. T.; Lay, P. a; Masters, a F.; Phillips, L. *J. Phys. Chem. B* **1999**, *103*, 6713.
- Chai, J.-D.; Head-Gordon, M. *Phys. Chem. Chem. Phys.* **2008**, *10*, 6615.
- Martin, J. M. L.; Sundermann, A. *J. Chem. Phys.* **2001**, *114*, 3408.
- Andrae, D.; Häußermann, U.; Dolg, M.; Stoll, H.; Preuß, H. *Theor. Chim. Acta* **1990**, *77*, 123.

- (46) Cossi, M.; Rega, N.; Scalmani, G.; Barone, V. *J. Comput. Chem.* **2003**, *24*, 669.
- (47) Scheytza, H.; Rademacher, O.; Reißig, H.-U. *Eur. J. Org. Chem.* **1999**, *1999*, 2373.
- (48) Hu, J.; Zhang, D.; Harris, F. W. *J. Org. Chem.* **2005**, *70*, 707.